



# Methyltrichlorosilane modified hydrophobic silica aerogels and their kinetic and thermodynamic behaviors

## Graphical Abstract

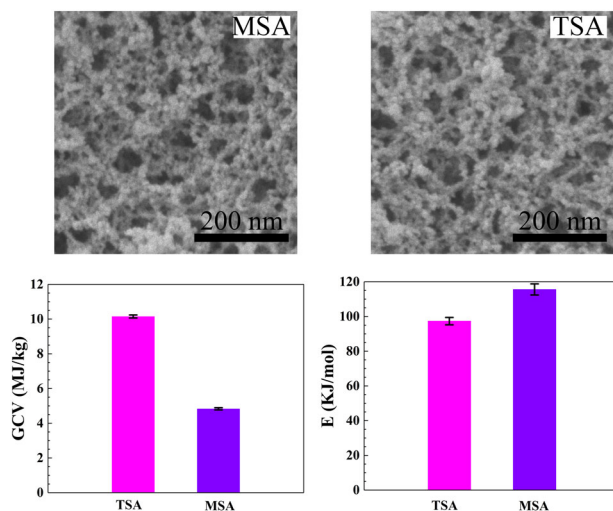
Wei Zhang<sup>1</sup> · Zhi Li<sup>1</sup> · Long Shi<sup>2</sup> · Zhicheng Li<sup>3</sup> · Yan Luo<sup>1</sup> · Qiong Liu<sup>1</sup> · Rui Huang<sup>1</sup>

Received: 25 September 2018 / Accepted: 13 November 2018 / Published online: 26 November 2018  
© Springer Science+Business Media, LLC, part of Springer Nature 2018

### Abstract

To reduce the flammability, hydrophobic silica aerogels (SAs) were modified by replacing commonly used trimethylchlorosilane (TMCS) with methyltrichlorosilane (MTCS). It was observed that the MTCS modified SAs (MSA) showed similar physicochemical properties to those TMCS modified SAs (TSA), including the density, thermal conductivity, hydrophobicity, and even thermal stability. However, the flammability of MSA was observed much lower than that of TSA, which was reflected by the significantly decreased gross calorific value (GCV). Furthermore, it was known from the kinetic and thermodynamic analyses that the pyrolysis of MSA became more difficult with the increasing conversion rate ( $\alpha$ ), which was evidenced by the fact that the apparent activation energy ( $E$ ) kept rising to about 194 kJ/mol during the whole pyrolysis. Based on the changed  $E$  along the time, the pyrolysis process could be divided into two stages, in which  $\alpha = 0.4$  was considered as the turning point. Those main thermodynamic parameters, including pre-exponential factor ( $A$ ) and the changes of enthalpy ( $\Delta H$ ) and entropy ( $\Delta S$ ), showed a quite consistent tendency with the  $E$ , whereas the change of Gibbs free energy ( $\Delta G$ ) almost kept unchanged. The research outcome of this study can provide a deep understanding of the pyrolysis process of SAs and render the public realize the thermal hazard risk of SAs.

### Graphical Abstract



✉ Zhi Li  
lizhi89@csu.edu.cn

<sup>1</sup> School of Resource and Safety Engineering, Central South University, Changsha 410083, P. R. China

<sup>2</sup> Civil and Infrastructure Engineering Discipline, School of Engineering, RMIT University, Melbourne, VIC 3000, Australia

<sup>3</sup> School of Materials Science and Engineering, Central South University, Changsha 410083, P. R. China

## Highlights

- MTCS replaced TMCS to modify silica aerogels to reduce the flammability.
- Gross calorific value of MTCS modified silica aerogels (MSA) decreased over 50%.
- Kinetic and thermodynamic behaviors of MSA were studied in detail.
- The pyrolysis of MSA was difficult to proceed along the time.
- This study provided a technical basis for the thermal hazards of silica aerogels.

**Keywords** Silica aerogels · Methyltrichlorosilanes · Thermal conductivity · Thermostability · Kinetics · Thermodynamics

## 1 Introduction

Due to the excellent physicochemical properties, silica aerogels (SAs) have been used in many areas, such as thermal insulation [1–6], oil/water separation [7–10], catalyst supports [11], and aerospace application [12]. Nowadays, SAs are usually considered as an excellent thermal insulation material with very wide adoption in the industries [13, 14]. As a thermal insulation material, the working condition with high temperature and thermal radiation are inevitable for those SAs. However, according to the literature review, the flammability studies of SAs are rarely explored. Only a few studies have been found focusing on the fire safety of polymer aerogels and their composites, such as cellulose aerogels [15], polyvinyl alcohol-based aerogel composites [16–18], fiber/aerogel composites [19], and polypropylene/SA composites [20]. The recent work by Ghazi Wakili directly investigated the reaction of ceramic fiber/aerogel composites to fire exposure [21], which inspired us and revealed the importance of studying the fire safety of aerogel materials. Commonly, SAs are considered as noncombustible [22], where the related evidence, such as experimental data, is lacking to justify it. Although the main

component is SiO<sub>2</sub>, there still exists some combustible ingredients in SAs and their roles in the overall flammability behaviors are still not well known. These then force us to take their flammability and thermal degradation into consideration in order to expand their applicability.

For hydrophobic SAs, the introduced organic functional groups by surface modification are the primary combustible components [23, 24], which are originally introduced to reduce the capillary tension during ambient pressure drying and provide the hydrophobicity. It is evident that those modifiers bring different organic functional groups onto SAs, which could deeply affect the thermal stability and flammability [25]. The commonly used modifiers are methyl silane and their derivatives, e.g., trimethylchlorosilane (TMCS) [26, 27]. Based on the quantity of methyl, those frequently adopted modifiers can be divided into three categories, including mono-, di-, and tri-functional organosilanes, as listed in Table 1, which can graft three, two, and one methyl groups, respectively, on SAs during the surface modification. For hydrophobic SAs, the more organic functional groups they are holding, the more hydrophobic and flammable the SAs are. Those modifiers not only increase the hydrophobicity for SAs, but also bring

**Table 1** A summary of three categories of frequently adopted modifiers

Types	Structure	R/Si	R <sub>n</sub> SiX <sub>4-n</sub> <sup>*</sup>
Mono-	$\begin{array}{c} \text{R} \\   \\ \text{R}-\text{Si}-\text{X} \\   \\ \text{R} \end{array}$	3	TMCS, HMDSO, HMDZ, etc.
Di-	$\begin{array}{c} \text{R} \\   \\ \text{R}-\text{Si}-\text{X} \\   \\ \text{X} \end{array}$	2	DMDCS, DMDMS, etc.
Tri-	$\begin{array}{c} \text{R} \\   \\ \text{X}-\text{Si}-\text{X} \\   \\ \text{X} \end{array}$	1	MTCS, MTMS, etc.

\*R represents the alkyl groups, usually –CH<sub>3</sub>; and X represents those hydrolysable groups, e.g., –OCH<sub>3</sub>, and halogen.

thermal hazards. Hence, a practical research question is whether it is possible to lower the flammability of SAs by reducing their organic functional content (e.g.,  $-\text{CH}_3$ ), but also maintaining those excellent physicochemical properties.

Inspired by the above thoughts, in this study, the commonly used mono-functional methyl silane (i.e., TMCS, with three  $-\text{CH}_3$  groups) was replaced with the tri-functional methyl silane (i.e., MTCS, with one  $-\text{CH}_3$  group) during the surface modification. The physicochemical tests were performed, together with the kinetic and thermodynamic analyses to identify the influences of the replacement. This study can be served as one of the pioneering attempts of the kinetic and thermodynamic analyses of SAs, which can then provide significant experimental evidence for the related statement and justification for the practical implementations.

## 2 Experimental methodology

### 2.1 Raw materials and preparation

The main chemical reagents, including tetraethylorthosilicate (TEOS), ethanol (EtOH), n-hexane, hydrochloric acid (HCl), and ammonia ( $\text{NH}_3 \cdot \text{H}_2\text{O}$ ) were CP grade from Sinopharm Chemical Reagent Co., Ltd (SCRC, China). Methyltrichlorosilane (MTCS) was purchased from Aladdin Reagent Co. Ltd., USA.

The classical acid–base catalyzed sol-gel and derivatization modification methods were adopted to synthesize hydrophobic SAs. The detailed preparation procedure can refer to our previous study [28], in which trimethylchlorosilane (TMCS) was used as the modifier. The as-prepared MTCS modified SAs were denoted as MSA and TMCS modified SAs were expressed as TSA in this study.

### 2.2 Characterization methods

The bulk density ( $\rho_b$ ) of SAs was calculated by the ratio of mass to volume, where the porosity was calculated [29]:

$$\text{Porosity} = \left(1 - \frac{\rho_b}{\rho_s}\right) \times 100\%, \quad (1)$$

in which,  $\rho_s$  is the skeletal density of the silica, usually considered as  $2200 \text{ kg/m}^3$ .

The hydrophobicity of prepared aerogels was characterized based on a contact angle meter (JC2000D1, Shanghai Zhongchen Instrument) by adding a water droplet of  $5 \mu\text{L}$  on the sample surface. The contact angle can be calculated

as follow [30]:

$$\theta = 2 \tan^{-1} \left( \frac{2h}{\Delta} \right), \quad (2)$$

where  $h$  is the height and  $\Delta$  is the base width of the water droplet.

The microstructures of MSA were observed by a double beam microscope (Helios Nanolab G3 UC, FEI Company). The nitrogen adsorption–desorption isotherms of MSA were tested at 77 K based on a Quadrasorb SI-3MP analyzer (Quantachrome, USA) and the pore parameters and pore size distribution (PSD) were calculated by Brunauer-Emmett-Teller (BET) and Barrett-Joyner-Halenda (BJH) methods. A thermal conductivity instrument (TC3000E, XIATECH, China) was employed to measure the thermal conductivity of MSA powders through transient hot-wire method. An oxygen bomb calorimeter (C3000, IKA, Germany) was used to obtain the gross calorific value (GCV) following ISO 1716: 2002. The thermal stability and kinetics behaviors were investigated by TG-DSC (SDT Q600, TA) under the heating rates of 5, 10, 15,  $20 \text{ }^\circ\text{C/min}$ , respectively, from room temperature to  $1000 \text{ }^\circ\text{C}$  in air.

### 2.3 Kinetic and thermodynamic methods

Generally, the variation of reaction rate as a function of temperature ( $T$ ) can be described as follow [31–33],

$$\frac{d\alpha}{dt} = A \exp\left(-\frac{E}{RT}\right) f(\alpha), \quad (3)$$

where  $A$ ,  $E$ ,  $\alpha$ , and  $R$  are the pre-exponential factor, apparent activation energy, conversion rate, and the universal gas constant ( $8.314 \text{ J/K/mol}$ ), respectively, and  $f(\alpha)$  is the reaction model.

Under non-isothermal conditions with constant heating rate, the temperature can be expressed as,

$$T = T_0 + \beta t, \quad (4)$$

where  $\beta$  is the heating rate and  $T_0$  is the initial temperature.

After combining Eq. (4), Eq. (3) can be given by,

$$\frac{d\alpha}{dT} = \frac{A}{\beta} \exp\left(-\frac{E}{RT}\right) f(\alpha). \quad (5)$$

Then, the variables  $\alpha$  and  $T$  can be separated for the integral. It is obtained:

$$G(\alpha) = \int_0^\alpha \frac{d\alpha}{f(\alpha)} = \frac{A}{\beta} \int_0^T \exp\left(-\frac{E}{RT}\right) dT, \quad (6)$$

**Table 2** A summary of kinetic models to calculate  $E^*$ 

Methods	Equation	Linear relationship
KAS method [34]	$\ln\left(\frac{\beta}{T^2}\right) = \ln\left(\frac{AR}{EG(\alpha)}\right) - \frac{E}{RT}$	$\ln(\beta/T^2) \sim 1/T$
OFW method [35]	$\ln \beta = \ln\left(\frac{AE}{RG(\alpha)}\right) - 5.3305 - 1.052 \frac{E}{RT}$	$\ln \beta \sim 1/T$
Friedman method [35]	$\ln\left(\beta \frac{d\alpha}{dT}\right) = \ln(Af(\alpha)) - \frac{E}{RT}$	$\ln(\beta d\alpha/dT) \sim 1/T$
Starink method [36]	$\ln\left(\frac{\beta}{T^{1.92}}\right) = C_s - 1.0008 \frac{E}{RT}$	$\ln(\beta/T^{1.92}) \sim 1/T$

\* $E$  can be calculated from the slope of the obtained linear relationship.

**Table 3** Comparisons of density, porosity, thermal conductivity, and contact angle between MSA and TSA

	Density (g/cm <sup>3</sup> )	Porosity (%)	Thermal conductivity (W/(m·K))	Contact angle (°)
MSA	0.13 ± 0.01	94.1 ± 0.5	0.0275 ± 0.0001	146 ± 1
TSA	0.11 ± 0.00	95.0 ± 0.2	0.0265 ± 0.0002	155 ± 2

where  $G(\alpha)$  denotes the right-side integral of Eq. (6).

Four frequently adopted methods, including Kissinger-Akahira-Sunose method (KAS), Ozawa-Wall-Flynn method (OFW), Friedman method and Starink method were listed in Table 2 and employed to calculate  $E$  in this study.

The pre-exponential factor ( $A$ ), the changes of enthalpy ( $\Delta H$ ), Gibbs free energy ( $\Delta G$ ), and the entropy ( $\Delta S$ ) can be obtained by Eqs. (7–10), respectively [37–39].

$$A = \beta E_{\alpha} \exp\left(\frac{E_{\alpha}}{RT_m}\right) / RT_m^2, \quad (7)$$

$$\Delta H = E_{\alpha} - RT_m, \quad (8)$$

$$\Delta G = E_{\alpha} + RT_m \ln\left(\frac{k_b T_m}{hA}\right), \quad (9)$$

$$\Delta S = \frac{\Delta H - \Delta G}{T_m}, \quad (10)$$

where  $k_b$  represents Boltzmann constant ( $1.381 \times 10^{-23}$  J/K),  $h$  is the Plank constant ( $6.626 \times 10^{-34}$  J·s),  $T_m$  denotes the peak temperature on DTG and  $T_{\alpha}$  is the temperature at a conversion of  $\alpha$ , respectively. Considering the fact that the heating rate of 10 °C/min was commonly used to test the thermal stability of SAs [40–43], the TG data obtained under the same heating rate were analyzed in the following content as the case to decide  $T_m$ , unless specified.

## 3 Results and discussion

### 3.1 Comparison between MSA and TSA

Comparisons of physicochemical features, including the density, porosity, thermal conductivity, and contact angle, between MSA and TSA are listed in Table 3. The density of MSA is about 0.13 g/cm<sup>3</sup>, which is slightly higher than that of TSA. Accordingly, the porosity of MSA is a little smaller than that of TSA, as seen in Table 3. It should be noticed that the porosities of both MSA and TSA reach up to 94%. As a thermal insulation material, a very low thermal

conductivity is fundamental. As seen in Table 3, the thermal conductivity of MSA is around 0.027 W/(m·K), which is very close to that of TSA, fulfilling the basic requirement of thermal insulation application. In general, the chemical composition and roughness of a material's surface show a great effect on the hydrophobicity [44]. The TSA and MSA both are hydrophobic with contact angles as high as ~155° and ~146°, respectively.

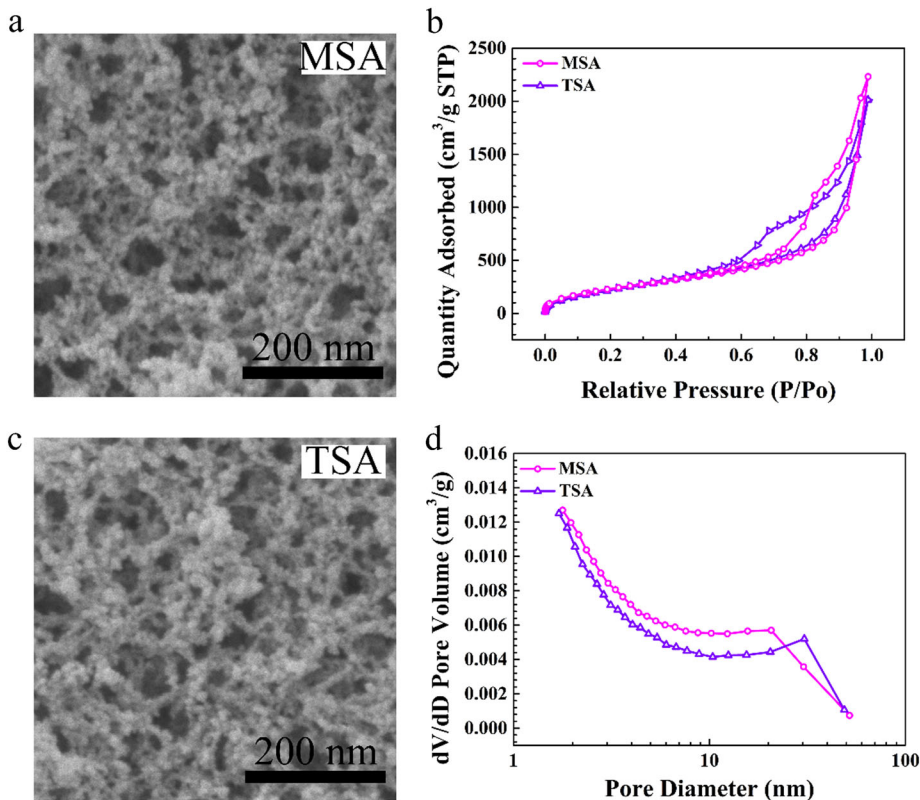
Following the above analyses, it is known that the physicochemical properties of MSA are very similar to those of typical TSA, including the density, thermal conductivity, and hydrophobicity. It is then indicated that MSA can also play an important role in the thermal insulation fields.

Figure 1a and c shows the microstructures of the MSA and TSA. These two kinds of SAs show similar nanoporous network structure, consisting of cross-linked and aggregated silica secondary nanoparticles. The nitrogen adsorption-desorption isotherms of typical MSA and TSA are exhibited in Fig. 1b, where their pore size distributions are presented in Fig. 1d. According to IUPAC [45], it is apparent that both samples exhibit typical characterizations of type IV isotherms, indicating the attribution of mesoporous materials. The existence of slit-like interparticle pores in the MSA and TSA has been demonstrated by the hysteresis loops of type H3 [46, 47]. As seen in Fig. 1d, the pore size distribution of MSA is very similar to that of the TSA, both of which contains micropores and mesopores. It is clearly seen in Table 4 that the pore parameters of the MSA and TSA are close to each other, which further confirms that the MSA has a similar microstructure to the TSA.

### 3.2 Thermostability analysis

It was observed from the TG-DSC curves in Fig. 2a, b, the MSA and TSA both have a sharp weight loss from 250 °C to 400 °C along with an obvious exothermic peak. This is commonly considered as the oxidative decomposition of  $-\text{CH}_3$  groups on the skeletons [48, 49]. In general, the thermostability of a material can be determined by the onset

**Fig. 1** Typical SEM images of MSA **a**, the  $N_2$  adsorption–desorption isotherms **b**, typical SEM images of TSA **c**, and the pore size distribution **d**



**Table 4** Pore parameters of the MSA and TSA

Samples	BET surface area (m <sup>2</sup> /g)	Pore volume (cm <sup>3</sup> /g)	Average pore size (nm)
MSA	889 ± 4	3.4 ± 0.3	12.8 ± 1.8
TSA	905 ± 6	3.1 ± 0.4	10.0 ± 2.6

**Table 5** Corresponding  $T_{onset}$ ,  $T_{peak}$  and  $-CH_3$  contents of the MSA and TSA

Samples	$T_{onset}$ (°C)	$T_{peak}$ (°C)	$-CH_3$ content (%)
MSA	242.35	276.54	5.28
TSA	243.56	275.16	9.26

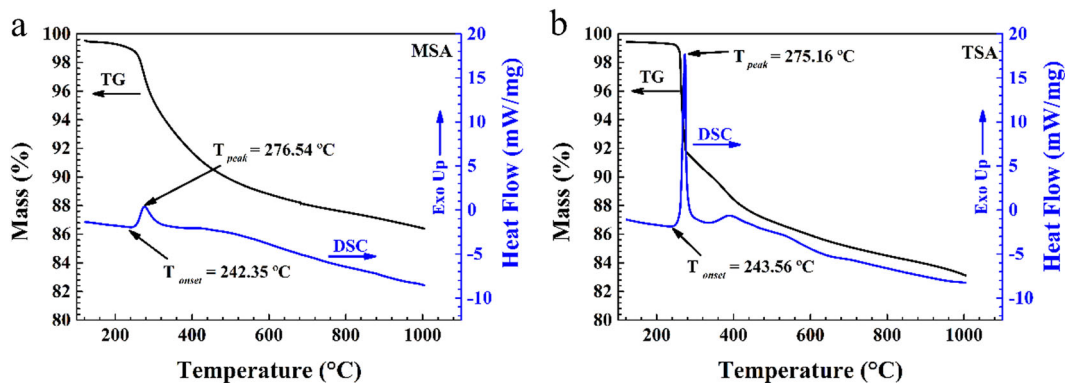


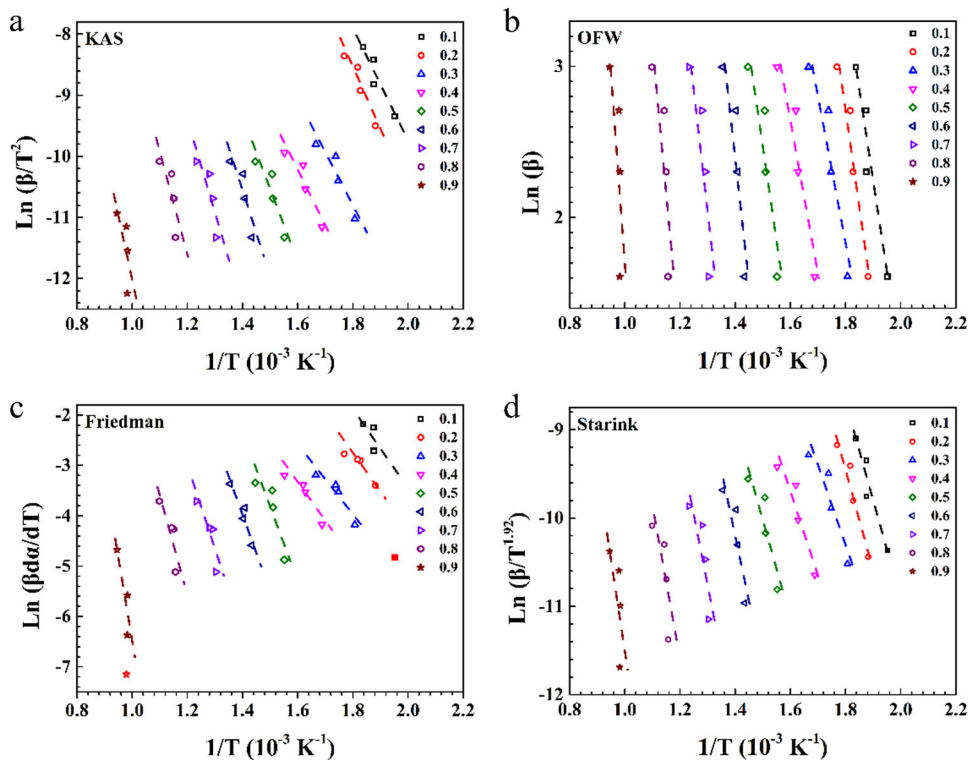
**Fig. 2** TG-DSC curves of the MSA **a** and TSA **b** under a heating rate of 10 °C/min in air

and peak temperatures of exothermic reactions, which are denoted as  $T_{onset}$  and  $T_{peak}$ , respectively. When the surrounding temperature exceeds  $T_{onset}$ , SAs lose the hydrophobicity gradually, leading to an absorption of the

moisture in air and subsequent deterioration of physical properties.

As seen in Table 5, the  $T_{onset}$  of MSA and TSA are 243.35 °C and 243.56 °C, respectively, whereas the  $T_{peak}$  of

**Fig. 3** Fitting lines of the kinetic parameters based on KAS method **a**, OFW method **b**, Friedman method **c**, and Starink method **d**



MSA and TSA are 276.54 °C and 275.16 °C, respectively. The very close  $T_{\text{onset}}$  and  $T_{\text{peak}}$  between MSA and TSA indicate that the two SAs have the similar thermal stability. Furthermore, the weight losses during the exothermic reaction can approximately be regarded as the  $-\text{CH}_3$  group. From the corresponding weight losses reflected by TG curves, the  $-\text{CH}_3$  content on MSA and TSA are calculated, which are about 5.28% and 9.26%, respectively. It demonstrates that the MSA possesses about 43% less  $-\text{CH}_3$  groups than that of TSA. The less the combustible organic groups are, the lower the thermal hazard of SAs is. Hence, compared to TSA, MSA shows a relatively lower thermal hazard potential.

### 3.3 Kinetic analysis

For conversion rates within 0.1–0.9, the least square method was employed to identify the optimal fitting lines for those four kinetic methods mentioned above. For the plots following these four kinetic methods, the  $Y$ -axis shows as  $\ln(\beta/T^2)$ ,  $\ln \beta$ ,  $\ln(\beta d\alpha/dT)$  and  $\ln(\beta/T^{1.92})$ , respectively, while all the  $X$ -axis are  $1/T$ . As illustrated in Fig. 3, the four points under the same  $\alpha$  all exhibit an obvious linear relationship. Furthermore, it can also be observed that the slopes of these fitting lines changes with a higher  $\alpha$ .

Figure 4 presents the apparent activation energy,  $E$ , along the increasing  $\alpha$ . It was observed that  $E$  obtained based on four methods are close to each other. The  $E$  shows an obvious increasing trend with a higher  $\alpha$ . It is indicated that

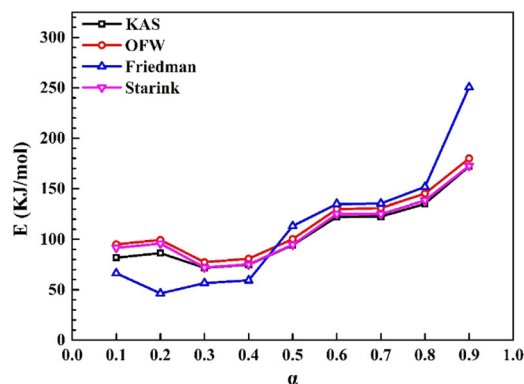


**Fig. 4**  $E$  along the increasing  $\alpha$  for the MSA

the decomposition of organic groups become more difficult along the process, which needs more energy to break those chemical bonds.

Based on the increasing  $E$ , it can be known that the pyrolysis of MSA is a multi-step process. Here, based on the variation of  $E$ , this pyrolysis process may be divided into two stages, where  $\alpha = 0.4$  can be considered as the turning point. The corresponding temperature ranges for these two stages can be seen in Table 6. At Stage I, the  $E$  nearly keeps constant, which may be mainly corresponding to the decomposition of organic groups (i.e.,  $-\text{CH}_3$ ) on the skeleton surface of MSA [50, 51]. At stage II,  $E$  shows an obvious rising trend, which may be because the organic

**Table 6** Two stages of the pyrolysis process for the MSA

$\alpha$	Stage I (0.1–0.4)	Stage II (0.4–0.9)
Temperature (°C)	100–310	310–800
Ave. $E$ (kJ/mol)	$77 \pm 4$	$139 \pm 8$

**Table 7** Thermodynamic data of the MSA under the heating rate of 10 °C/min

$\alpha$	$A$ (s <sup>-1</sup> )	$\Delta H$ (kJ/mol)	$\Delta G$ (kJ/mol)	$\Delta S$ (J/K/mol)
0.1	$5.79 \times 10^5$	79.15	159.87	-147.93
0.2	$3.88 \times 10^5$	77.43	159.96	-151.27
0.3	$2.09 \times 10^4$	64.93	160.72	-175.54
0.4	$4.27 \times 10^4$	67.97	160.52	-169.61
0.5	$2.89 \times 10^7$	96.06	159.04	-115.41
0.6	$1.58 \times 10^{10}$	123.55	157.94	-63.03
0.7	$1.71 \times 10^{10}$	123.89	157.93	-62.37
0.8	$4.27 \times 10^{11}$	138.03	157.45	-35.60
0.9	$4.65 \times 10^{16}$	189.25	156.06	60.83

groups in the skeletons need more energy to support the decomposition. Besides, during this stage, the condensation reaction between Si–OH groups, oxidized from Si–CH<sub>3</sub> groups, would launch and produce water, which also can result in an increase of  $E$  [52].

### 3.4 Thermodynamic analysis

The average  $E$  calculated from the above four methods were employed to obtain thermodynamic data, i.e., pre-exponential factor ( $A$ ), the changes of enthalpy ( $\Delta H$ ), Gibbs free energy ( $\Delta G$ ), and entropy ( $\Delta S$ ). The results have been listed in Table 7.

As seen in Table 7, for  $\alpha$  within 0.1–0.9,  $A$  is located in a wide range of  $2.09 \times 10^4$ – $4.65 \times 10^{16}$  s<sup>-1</sup>, which is consistent with the variation trend of  $E$ . It is noted that for  $\alpha = 0.2$ – $0.4$ , the minimal  $A$  appears, just corresponding to the minimum of  $E$ , which should be speculated to correlate with the fastest pyrolysis rate, i.e., the exothermic peak. At  $T_{\text{peak}}$ , the minimal  $E$  suggests that less energy can activate the reactive molecules, leading to an increasing effective collision, in spite of a lower  $A$ . Specifically speaking, the main reaction during the pyrolysis is the oxidation of Si–CH<sub>3</sub> groups on the surface skeletons of MSA according to our previous study [50]. Along with the pyrolysis proceeding, –CH<sub>3</sub> groups are decreased, which would need more energy to activate certain complex reactions, resulting in an increasing  $E$  and  $A$ .

It is known that the variation of  $\Delta H$  is the enthalpy difference between the activated complexes and reactants [53]. As seen in Table 7,  $\Delta H$  increases with a higher  $\alpha$  and reaches up to 189.25 kJ/mol. Thus, it means that more

energy needs to be introduced into the reaction system to break chemical bonds so that the pyrolysis can keep proceeding. Furthermore, it was observed that the  $\Delta H$  is quite consistent with the  $E$  during the pyrolysis process.

It is also known that Gibbs free energies state the favorability of reactions regarding the first and second laws of thermodynamics [54]. Furthermore, the increased total energy of reaction system at the way of reagents and the formation of the activated complex can be reflected by the change of the Gibbs free energy ( $\Delta G$ ) [53]. As seen in Table 7,  $\Delta G$  nearly keeps unchanged for various  $\alpha$ , just ranging from 156 kJ/mol to 161 kJ/mol. That is to say, with respect to the overall energy required in the pyrolysis process, no obvious difference is observed at different stages. Besides, the higher  $\Delta G$ , more than zero, indicates that the whole pyrolysis process can not happen spontaneously without external energy supply.

Entropy ( $\Delta S$ ), as a state function, reflects the disorder degree of the reaction system [53]. The negative values of  $\Delta S$  suggests that the degree of disorder of products is lower than the initial reactants via absorbing external energies for bond dissociations [54]. For a lower  $\Delta S$ , the reactivity of the material is low, which is accompanied with the increasing time of forming activated complexes [55]. On the contrary, for a higher  $\Delta S$ , the reactivity is high and the system can react relatively fast to generate more activated complexes in a short time period [55]. As listed in Table 7,  $\Delta S$  has the same tendency with  $E$ , with an increase from -176 to 61 J/K/mol, which suggests that the reactivity of the reaction system is increasing. In spite of that, the average  $\Delta S$  during the overall pyrolysis is about -96 J/K/mol, indicating that the reactivity of the system maintains at a low level during the whole-pyrolysis process.

From the above analyses, it can be concluded that the pyrolysis of MSA is difficult to proceed along the time based on the increased  $E$  and the positive  $\Delta G$ . All these obtained thermodynamic data could put forward our understanding of the pyrolysis process of MSA.

### 3.5 GCV and thermal hazard comparison between MSA and TSA

The total heat release of a material under complete combustion can be reflected by GCV [56–59]. Figure 5 shows the test process of GCV of as-prepared MSA. To prevent the MSA from splattering out of the crucible during the combustion process, we put them into a PE-bag and measure them together. The finally obtained GCV for the MSA were obtained by subtracting the GCV of the PE-bag.

As illustrated in Fig. 6a, it can be seen that the GCV of MSA is about 4.8 MJ/kg which decreases over 50% when compared to that of TSA (~10 MJ/kg). The less GCV of MSA suggests the potential thermal hazard is lower than

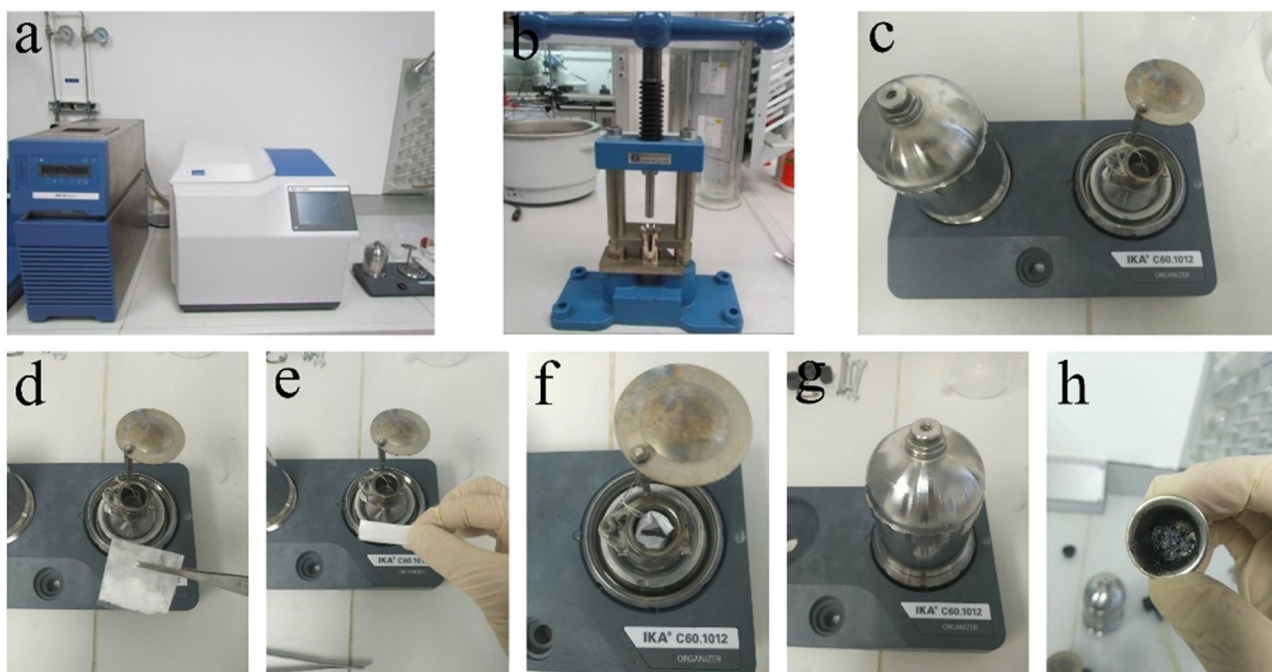
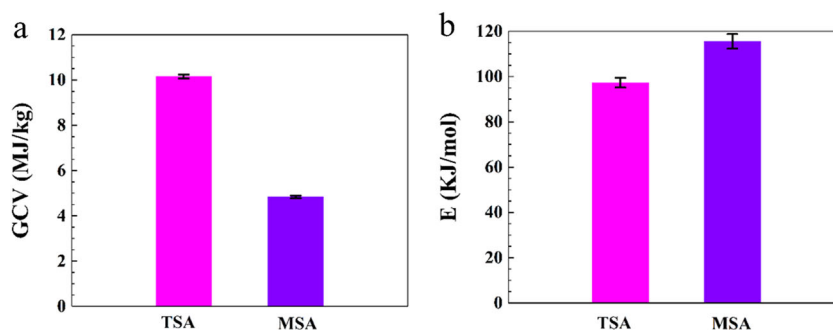


**Fig. 5** Test process of GCV of the MSA, **a** a calorimeter C3000, IKA, **b** a pelleting press machine, **c** an oxygen bomb, **d** a PE-bag, **e–g** moving the PE-bag filled with samples into an oxygen bomb and **h** a crucible with the combustion products inside

**Fig. 6** **a** GCV of the TSA and MSA, and **b** the average  $E$  of the TSA and MSA, in which the average  $E$  of the TSA comes from ref. [24]



that of TSA. This change is largely due to the reduction in  $-\text{CH}_3$  content on the MSA which has been addressed above in the thermal stability section. Furthermore, as presented in Fig. 6b, the average  $E$  of TSA is less than that of MSA, which indicates that TSA can reach the activated reaction status more easily and the required reaction temperature is lower when compared with the MSA. Namely, the tendency or probability of pyrolysis occurring on TSA is higher than that of MSA. Thus, it can be further known that the MSA holds better fire retardancy and lower potential thermal hazard when compared with the TSA.

## 4 Conclusions

In this study, hydrophobic silica aerogels (SAs) were modified by replacing commonly used trimethylchlorosilane (TMCS) with methyltrichlorosilane (MTCS),

where experiments were also conducted to investigate their physicochemical, kinetic, and thermodynamic behaviors.

The experimental results showed that the density, hydrophobicity, thermal conductivity, and thermostability of MTCS modified SAs (MSA) were close to those of TMCS modified SAs (TSA), which demonstrated that MSA could fulfill an excellent performance of thermal insulation. It was also known from the experiments that the gross calorific value (GCV) of MSA was reduced by over 50% when compared to that of the TSA, which indicated that the tri-functional methyl silane modified SAs could effectively lower the thermal hazard by reducing organic groups ( $-\text{CH}_3$ ).

Furthermore, the obtained apparent activation energy ( $E$ ) showed an increasing trend with a higher conservation ( $\alpha$ ), where  $\alpha = 0.4$  could be regarded as the turning point for the division of two stages. As seen from the overall pyrolysis process, the pre-exponential factor ( $A$ ), the changes of enthalpy ( $\Delta H$ ) and entropy ( $\Delta S$ ) all presented an increasing



trend with a higher  $\alpha$ , which suggested that the pyrolysis of MSA was difficult to proceed along the time. The change of Gibbs free energy ( $\Delta G$ ) indicated that the pyrolysis of MSA can not happen spontaneously without external energy supply. These research outcomes of this study can provide a technical basis for the thermal hazards of silica aerogels.

**Acknowledgements** This work was supported by the Fundamental Research Funds for the Central Universities (grant number 202501003, 202045001 and 502211841).

## Compliance with ethical standards

**Conflict of interest** The authors declare that they have no conflict of interest.

## References

1. Koebel M, Rigacci A, Achard P (2012) Aerogel-based thermal superinsulation: an overview. *J Sol-Gel Sci Technol* 63:315–339. <https://doi.org/10.1007/s10971-012-2792-9>
2. Liang Y, Wu H, Huang G, Yang J, Wang H (2017) Thermal performance and service life of vacuum insulation panels with aerogel composite cores. *Energy Build* 154:606–617. <https://doi.org/10.1016/j.enbuild.2017.08.085>
3. Yang J, Wu H, Huang G, Liang Y, Liao Y (2017) Modeling and coupling effect evaluation of thermal conductivity of ternary opacifier/fiber/aerogel composites for super-thermal insulation. *Mater Des* 133:224–236. <https://doi.org/10.1016/j.matdes.2017.07.056>
4. Zhu P, Zheng M, Zhao S, Wu J, Xu H, Novel A (2016) Environmental route to ambient pressure dried thermal insulating silica aerogel via recycled coal gangue. *Adv Mater Sci Eng* 2016:1–9. <https://doi.org/10.1155/2016/9831515>
5. Stahl T, Brunner S, Zimmermann M, Wakili KGhazi (2012) Thermo-hygric properties of a newly developed aerogel based insulation rendering for both exterior and interior applications. *Energy Build* 44:114–117. <https://doi.org/10.1016/j.enbuild.2011.09.041>
6. Galliano R, Ghazi Wakili K, Stahl T, Binder B, Daniotti B (2016) Performance evaluation of aerogel-based and perlite-based prototyped insulations for internal thermal retrofitting: HMT model validation by monitoring at demo scale. *Energy Build* 126:275–286. <https://doi.org/10.1016/j.enbuild.2016.05.021>
7. Reynolds JohnG, Coronado PaulR, Hrubesh LawrenceW (2001) Hydrophobic aerogels for oil-spill clean up – synthesis and characterization. *J Non-Cryst Solids* 292:127–137. [https://doi.org/10.1016/S0022-3093\(01\)00882-1](https://doi.org/10.1016/S0022-3093(01)00882-1)
8. He S, Cheng X, Li Z, Shi X, Yang H, Zhang H (2016) Green and facile synthesis of sponge-reinforced silica aerogel and its pumping application for oil absorption. *J Mater Sci* 51:1292–1301. <https://doi.org/10.1007/s10853-015-9427-9>
9. Wang Q, Yu M, Chen G, Chen Q, Tian J (2017) Robust fabrication of fluorine-free superhydrophobic steel mesh for efficient oil/water separation. *J Mater Sci* 52:2549–2559. <https://doi.org/10.1007/s10853-016-0548-6>
10. Yu Y, Wu X, Fang J (2015) Superhydrophobic and superoleophilic “sponge-like” aerogels for oil/water separation. *J Mater Sci* 50:5115–5124. <https://doi.org/10.1007/s10853-015-9034-9>
11. Wu J, Yang H (2013) Platinum-based oxygen reduction electrocatalysts. *Acc Chem Res* 46:1848–1857. <https://doi.org/10.1021/a300359w>
12. Randall JP, Meador MAB, Jana SC (2011) Tailoring mechanical properties of aerogels for aerospace applications. *ACS Appl Mater Interfaces* 3:613–626. <https://doi.org/10.1021/am200007n>
13. Maghsoudi K, Motahari S (2018) Mechanical, thermal, and hydrophobic properties of silica aerogel-epoxy composites. *J Appl Polym Sci* 135:45706. <https://doi.org/10.1002/app.45706>
14. Ma J, Ye F, Yang C, Ding J, Lin S, Zhang B, Liu Q (2017) Heat-resistant, strong alumina-modified silica aerogel fabricated by impregnating silicon oxycarbide aerogel with boehmite sol. *Mater Des* 131:226–231. <https://doi.org/10.1016/j.matdes.2017.06.036>
15. Han Y, Zhang X, Wu X, Lu C (2015) Flame retardant, heat insulating cellulose aerogels from waste cotton fabrics by in situ formation of magnesium hydroxide nanoparticles in cellulose gel nanostructures. *ACS sustain. Chem Eng* 3:1853–1859. <https://doi.org/10.1021/acssuschemeng.5b00438>
16. Wang L, Sánchez-Soto M, Maspoeh ML (2013) Polymer/clay aerogel composites with flame retardant agents: mechanical, thermal and fire behavior. *Mater Des* 1980–2015 52:609–614. <https://doi.org/10.1016/j.matdes.2013.05.096>
17. Chen H-B, Wang Y-Z, Schiraldi DA (2014) Preparation and flammability of poly(vinyl alcohol) composite aerogels. *ACS Appl Mater Interfaces* 6:6790–6796. <https://doi.org/10.1021/a500583x>
18. Wang Y-T, Liao S-F, Shang K, Chen M-J, Huang J-Q, Wang Y-Z, Schiraldi DA (2015) Efficient approach to improving the flame retardancy of poly(vinyl alcohol)/clay aerogels: incorporating piperazine-modified ammonium polyphosphate. *ACS Appl Mater Interfaces* 7:1780–1786. <https://doi.org/10.1021/am507409d>
19. Siligardi C, Miselli P, Francia E, Gualtieri MLassinantti (2017) Temperature-induced microstructural changes of fiber-reinforced silica aerogel (FRAB) and rock wool thermal insulation materials: a comparative study. *Energy Build* 138:80–87. <https://doi.org/10.1016/j.enbuild.2016.12.022>
20. Motahari S, Motlagh GH, Moharramzadeh A (2015) Thermal and flammability properties of polypropylene/silica aerogel composites. *J Macromol Sci Part B* 54:1081–1091. <https://doi.org/10.1080/00222348.2015.1078619>
21. Ghazi Wakili K, Remhof A (2017) Reaction of aerogel containing ceramic fibre insulation to fire exposure: reaction of aerogel containing insulation to fire. *Fire Mater* 41:29–39. <https://doi.org/10.1002/fam.2367>
22. Kashiwagi T, Gilman JW, Butler KM, Harris RH, Shields JR, Asano A (2000) Flame retardant mechanism of silica gel/silica. *Fire Mater* 24:277–289. [https://doi.org/10.1002/1099-1018\(200011/12\)24:6<277::AID-FAM746>3.0.CO;2-A](https://doi.org/10.1002/1099-1018(200011/12)24:6<277::AID-FAM746>3.0.CO;2-A)
23. Li Z, Cheng X, Gong L, Liu Q, Li S (2018) Enhanced flame retardancy of hydrophobic silica aerogels by using sodium silicate as precursor and phosphoric acid as catalyst. *J Non-Cryst Solids* 481:267–275. <https://doi.org/10.1016/j.jnoncrysol.2017.10.053>
24. Li Z, Cheng X, Shi L, He S, Gong L, Li C, Zhang H (2016) Flammability and oxidation kinetics of hydrophobic silica aerogels. *J Hazard Mater* 320:350–358. <https://doi.org/10.1016/j.jhazmat.2016.07.054>
25. Mahadik SA, Pedraza F, Parale VG, Park H-H (2016) Organically modified silica aerogel with different functional silylating agents and effect on their physico-chemical properties. *J Non-Cryst Solids* 453:164–171. <https://doi.org/10.1016/j.jnoncrysol.2016.08.035>
26. Rao AV, Pajonk GM, Bhagat SD, Barbooux P (2004) Comparative studies on the surface chemical modification of silica aerogels based on various organosilane compounds of the type  $R_nSiX_{4-n}$ . *J Non-Cryst Solids* 350:216–223. <https://doi.org/10.1016/j.jnoncrysol.2004.06.034>
27. Mahadik DB, Rao AV, Rao AP, Wagh PB, Ingale SV, Gupta SC (2011) Effect of concentration of trimethylchlorosilane (TMCS) and hexamethyldisilazane (HMDZ) silylating agents on surface

- free energy of silica aerogels. *J Colloid Interface Sci* 356:298–302. <https://doi.org/10.1016/j.jcis.2010.12.088>
28. Li Z, Cheng X, He S, Shi X, Yang H (2015) Characteristics of ambient-pressure-dried aerogels synthesized via different surface modification methods. *J Sol-Gel Sci Technol* 76:138–149. <https://doi.org/10.1007/s10971-015-3760-y>
  29. He F, Zhao H, Qu X, Zhang C, Qiu W (2009) Modified aging process for silica aerogel. *J Mater Process Technol* 209:1621–1626. <https://doi.org/10.1016/j.jmatprotec.2008.04.009>
  30. Nadargi DY, Kalesh RR, Rao AV (2009) Rapid reduction in gelation time and impregnation of hydrophobic property in the tetraethoxysilane (TEOS) based silica aerogels using NH<sub>4</sub>F catalyzed single step sol–gel process. *J Alloy Compd* 480:689–695. <https://doi.org/10.1016/j.jallcom.2009.02.027>
  31. Turmanova SC, Genieva SD, Dimitrova AS, Vlaev LT (2008) Non-isothermal degradation kinetics of filled with rise husk ash polypropylene composites. *Express Polym Lett* 2:133–146. <https://doi.org/10.3144/expresspolymlett.2008.18>
  32. Chen Y, Wang Q (2007) Thermal oxidative degradation kinetics of flame-retarded polypropylene with intumescent flame-retardant master batches in situ prepared in twin-screw extruder. *Polym Degrad Stab* 92:280–291. <https://doi.org/10.1016/j.polymdegradstab.2006.11.004>
  33. Vlaev LT, Georgieva VG, Genieva SD (2007) Products and kinetics of non-isothermal decomposition of vanadium(IV) oxide compounds. *J Therm Anal Calorim* 88:805–812. <https://doi.org/10.1007/s10973-005-7149-y>
  34. Ozawa T (1992) Estimation of activation energy by isoconversion methods. *Thermochim Acta* 203:159–165. [https://doi.org/10.1016/0040-6031\(92\)85192-X](https://doi.org/10.1016/0040-6031(92)85192-X)
  35. M Sharara, S Sadaka (2014) Thermogravimetric analysis of swine manure solids obtained from farrowing, and growing-finishing farms, *J Sustain Bioenergy Syst* 2014. <https://doi.org/10.4236/jsbs.2014.41008>
  36. Starink MJ (1996) A new method for the derivation of activation energies from experiments performed at constant heating rate. *Thermochim Acta* 288:97–104. [https://doi.org/10.1016/S0040-6031\(96\)03053-5](https://doi.org/10.1016/S0040-6031(96)03053-5)
  37. Xu Y, Chen B (2013) Investigation of thermodynamic parameters in the pyrolysis conversion of biomass and manure to biochars using thermogravimetric analysis. *Bioresour Technol* 146:485–493. <https://doi.org/10.1016/j.biortech.2013.07.086>
  38. Maia AAD, de Moraes LC (2016) Kinetic parameters of red pepper waste as biomass to solid biofuel. *Bioresour Technol* 204:157–163. <https://doi.org/10.1016/j.biortech.2015.12.055>
  39. Kim YS, Kim YS, Kim SH (2010) Investigation of thermodynamic parameters in the thermal decomposition of plastic waste –waste lube oil compounds. *Environ Sci Technol* 44:5313–5317. <https://doi.org/10.1021/es101163e>
  40. Wu X, Fan M, Shen X, Cui S, Tan G (2018) Silica aerogels formed from soluble silicates and methyl trimethoxysilane (MTMS) using CO<sub>2</sub> gas as a gelation agent. *Ceram Int* 44:821–829. <https://doi.org/10.1016/j.ceramint.2017.10.005>
  41. Cheng X, Li C, Shi X, Li Z, Gong L, Zhang H (2017) Rapid synthesis of ambient pressure dried monolithic silica aerogels using water as the only solvent. *Mater Lett* 204:157–160. <https://doi.org/10.1016/j.matlet.2017.05.107>
  42. He S, Sun G, Cheng X, Dai H, Chen X (2017) Nanoporous SiO<sub>2</sub> grafted aramid fibers with low thermal conductivity. *Compos Sci Technol* 146:91–98. <https://doi.org/10.1016/j.compscitech.2017.04.021>
  43. Gurav JL, Rao AV, Rao AP, Nadargi DY, Bhagat SD (2009) Physical properties of sodium silicate based silica aerogels prepared by single step sol–gel process dried at ambient pressure. *J Alloy Compd* 476:397–402. <https://doi.org/10.1016/j.jallcom.2008.09.029>
  44. Mahadik DB, Venkateswara Rao A, Parale VG, Kavale MS, Wagh PB, Ingale SV, Gupta SC (2011) Effect of surface composition and roughness on the apparent surface free energy of silica aerogel materials. *Appl Phys Lett* 99:104104. <https://doi.org/10.1063/1.3635398>
  45. Sing KSW (1985) Reporting physisorption data for gas/solid systems—with special reference to the determination of surface area and porosity. *Pure Appl Chem* 57:603–619. <https://doi.org/10.1351/pac198557040603>
  46. Rojas F, Kornhauser I, Felipe C, Esparza JM, Cordero S, Dominguez A, Riccardo JL (2002) Capillary condensation in heterogeneous mesoporous networks consisting of variable connectivity and pore-size correlation. *Phys Chem Chem Phys* 4:2346–2355. <https://doi.org/10.1039/b108785a>
  47. Lermontov SA, Malkova AN, Yurkova LL, Straumal EA, Gubanova NN, Baranchikov AY, Ivanov VK (2014) Diethyl and methyl-tert-butyl ethers as new solvents for aerogels preparation. *Mater Lett* 116:116–119. <https://doi.org/10.1016/j.matlet.2013.10.080>
  48. Li Z, Cheng X, He S, Shi X, Yang H, Zhang H (2016) Tailoring thermal properties of ambient pressure dried MTMS/TEOS coprecursor aerogels. *Mater Lett* 171:91–94. <https://doi.org/10.1016/j.matlet.2016.02.025>
  49. Wu G, Yu Y, Cheng X, Zhang Y (2011) Preparation and surface modification mechanism of silica aerogels via ambient pressure drying. *Mater Chem Phys* 129:308–314. <https://doi.org/10.1016/j.matchemphys.2011.04.003>
  50. Li Z, Cheng X, Shi L, He S, Gong L, Li C, Zhang H (2016) Flammability and oxidation kinetics of hydrophobic silica aerogels. *J Hazard Mater* 320:350–358. <https://doi.org/10.1016/j.jhazmat.2016.07.054>
  51. S He, Y Huang, G Chen, M Feng, H Dai, B Yuan, X Chen (2018) Effect of heat treatment on hydrophobic silica aerogel. *J Hazard Mater*. <https://doi.org/10.1016/j.jhazmat.2018.08.087>
  52. Zhuravlev LT (2000) The surface chemistry of amorphous silica. Zhuravlev model. *Colloids Surf Physicochem Eng Asp* 173:1–38. [https://doi.org/10.1016/S0927-7757\(00\)00556-2](https://doi.org/10.1016/S0927-7757(00)00556-2)
  53. Yuan X, He T, Cao H, Yuan Q (2017) Cattle manure pyrolysis process: kinetic and thermodynamic analysis with isoconversional methods. *Renew Energy* 107:489–496. <https://doi.org/10.1016/j.renene.2017.02.026>
  54. Kim YS, Kim YS, Kim SH (2010) Investigation of thermodynamic parameters in the thermal decomposition of plastic waste –waste lube oil compounds. *Environ Sci Technol* 44:5313–5317. <https://doi.org/10.1021/es101163e>
  55. Ruvolo-Filho A, Curti PS (2006) Chemical kinetic model and thermodynamic compensation effect of alkaline hydrolysis of waste poly(ethylene terephthalate) in nonaqueous ethylene glycol solution. *Ind Eng Chem Res* 45:7985–7996. <https://doi.org/10.1021/ie060528y>
  56. Matin SS, Chelgani SC (2016) Estimation of coal gross calorific value based on various analyses by random forest method. *Fuel* 177:274–278. <https://doi.org/10.1016/j.fuel.2016.03.031>
  57. Llorente MJF, García JEC (2008) Suitability of thermo-chemical corrections for determining gross calorific value in biomass. *Thermochim Acta* 468:101–107. <https://doi.org/10.1016/j.tca.2007.12.003>
  58. Mancini M, Rinnan A, Pizzi A, Toscano G (2018) Prediction of gross calorific value and ash content of woodchip samples by means of FT-NIR spectroscopy *Fuel Process Technol* 169:77–83. <https://doi.org/10.1016/j.fuproc.2017.09.021>
  59. Rhén C (2004) Chemical composition and gross calorific value of the above-ground biomass components of young *Picea abies*, Scand. *J For Res* 19:72–81. <https://doi.org/10.1080/02827580310019185>